Check for updates

Synthesis of CeO$_2$-NPs by chemical and biological methods and their photocatalytic, antibacterial and in vitro antioxidant activity

A. Muthuvel[1] · M. Jothibas[1] · C. Manoharan[2] · S. Johnson Jayakumar[1]

Abstract

In the present study, biosynthesized CeO$_2$-NPs using *Solanum nigrum* leaf extract were compared with chemically synthesized one. The synthesized CeO$_2$-NPs were characterized by UV–Vis, XRD, DLS, ZP, HR-TEM, FT-IR and PL techniques. UV–visible spectrum showed absorption peak in the range of 326–355 nm. DLS studies exposed that the average size of CeO$_2$-NPs was around 45 nm and the obtained zeta potential value of -25.83 mV for CeO$_2$-NPs indicated moderate stability of biosynthesized nanoparticles. HR-TEM images revealed the spherical morphology of the biosynthesized CeO$_2$-NPs with the size of 20 nm and selected area diffraction pattern revealed the polycrystalline nature of CeO$_2$-NPs, which was consistent with the XRD result. FT-IR analysis also confirmed the presence of metal oxide. The synthesized CeO$_2$-NPs exhibited potential photocatalytic activity towards the degradation of methylene blue dye upon exposure to sunlight irradiation. The degradation efficiencies of Chem and biosynthesized CeO$_2$-NPs towards methylene blue dye were 78.14 and 94.58%, respectively. In addition, antibacterial and antioxidant activity of synthesized CeO$_2$-NPs is evaluated. The biosynthesized CeO$_2$-NPs possess highest antibacterial activity against Gram-negative *Escherichia coli* (22 ± 0.3 mm) and Gram-positive *Bacillus subtilis* (21 ± 0.4 mm) at 100 μl. The biosynthesized CeO$_2$-NPs exhibited greater inhibition on DPPH radical IC$_{50}$ μg/ml value which was 139 ± 45, while it was 131 ± 21 for hydroxyl radical. The present work demonstrated an eco-friendly preparation of CeO$_2$-NPs with good photocatalytic, antibacterial and antioxidant properties.

Keywords Chem CeO$_2$-NPs · Biosynthesized CeO$_2$-NPs · *S. nigrum* · Photocatalytic · Antibacterial · Antioxidant activity

✉ M. Jothibas
  jothibas1980@gmail.com

1 PG and Research Department of Physics, T.B.M.L. College, Porayar, Tamil Nadu 609307, India

2 Department of Physics, Annamalai University, Annamalai Nagar, Tamil Nadu 608002, India

Introduction

Metal and metal oxide nanoparticles (NPs) are developing as a potential candidate in the field of nanoscience and nanotechnology. The size and shape of metallic nanoparticles play a major role with their physical, chemical, electrical and optical properties. The applications like sensors, catalysis, antibacterial, luminescent materials, etc., are found in metallic nanoparticles [1, 2]. The metal oxide nanoparticles such as CeO_2, ZnO, CuO, TiO_2, SnO_2 and CoO are widely exploited because of their special physicochemical properties but these are cost-effective, simple and environment friendly [3, 4]. Among several metal oxide nanoparticles, cerium oxide (CeO_2, also known as ceria) is one of the rare reactive metals available on the earth which has great importance in recent years. It has special characteristics, like high stability at extreme temperature, UV absorption ability, high hardness and reactivity [5]. The various applications of CeO_2-NPs are sensor, sunscreen cosmetics, solid oxide fuel cells and antibacterial application including labelling, advanced drug delivery, photothermal therapy, tissue/tumour imaging and molecular diagnostic and most recently in eye disorder and disease treatments [6–9]. CeO_2-NPs have been included into many industrial products [10]. It is believed that the antimicrobial activity of the CeO_2-NPs might be either due to the generation of hydrogen peroxide or due to the electrostatic binding of the particles on the microbial surface. Conventional CeO_2-NPs are synthesized by various physical and chemical methods, such as sol–gel methods [11], flame spray pyrolysis [12], hydrothermal synthesis [13], microwave-assisted heating routes and sonochemical [14] solid-state reactions at room temperature [15], homogeneous precipitation with urea or hexamethylenetetramine [16], co-precipitation, and so on [17]. However, most of these techniques are not environment friendly. The toxic chemical by product makes CeO_2-NPs inappropriate for use in biomedical application. Since it is complex, it needs small particles and is expensive to manufacture. Hence, the preparation technique is shifted towards 'green' chemistry and bioprocess approach. Nowadays the green synthesis route is highly relevant as it is nontoxic, cost-effective, decreasing/totally eliminates the use and production of substance hazardous to human health and environment biocompatible reducing agents for the synthesis of CeO_2-NPs [18]. Various biological systems such as plants, bacteria, honey, egg white and fungal extracellular compounds are being continuously investigated for the synthesis of CeO_2-NPs. Among them, the use of extracts obtained from plant materials attracts the interest of the scientific community due to their biocomponents, which act as capping and reducing agent and provide to prepare a nanocrystalline, metal oxide nanoparticles in different sizes and morphologies [19]. They help to remove completely the cell structure. Arumugam et al. reported that the *Gloriosa superba* leaf extract-mediated CeO_2-NPs had shown efficient antimicrobial activity [20]. Venkatesh et al. reported that the *Fusarium solani*-mediated biosynthesized CeO_2-NPs were active against clinically isolated human pathogens, *P. aeruginosa* as well as *K. pneumonia* [21]. In single step, biosynthesis of CeO_2-NPs is presented by reduction of cerium chloride ($CeCl_3$) at room temperature with *Solanum nigrum* leaf

extract. *Solanum nigrum* (*S. nigrum*) is a species in the family Solanaceae. In India, the traditional medicine system uses *S. nigrum* in herbaceous perennial plant for its anti-inflammatory, anti-ulcerogenic, anti-tumorigenic and antioxidant characteristics [22] since it could withstand elevated important metal concentration in contaminated soils. The phytochemical considers uncovering the nearness of solasonine, alkaloids and solamargine that produce starch glycone solasodine, which is bioactive. It is in great demand in the pharmaceutical industry, since it has tolerance to an adverse environment and can fill the gap of known hyperactive accumulating plants.

In the present work, chemically synthesized CeO₂-NPs are compared with the biosynthesized CeO₂-NPs using aqueous leaf extract of *S. nigrum* (0.5:1, 1:1, 1.5:1 and 2:1 *v/v*) for various percentages. The *S. nigrum* leaf extract is used as a reducing and capping agent. The synthesized CeO₂-NPs are characterized by using UV–visible spectroscopy, XRD, DLS, ZP, HR-TEM, FT-IR and PL technique. The productivity of CeO₂-NPs as a photocatalyst for the degradation of methylene blue dye and antibacterial and their antioxidant activity by DPPH assay is studied.

Experimental sections

Materials

Fresh leaves of *S. nigrum* were collected from rural regions of Porayar, Tamil Nadu, India. Cerium chloride (CeCl₃) (99.9%) was from Sigma-Aldrich, Bangalore, India, and was used as received. All the bacterial cultures, viz. *Bacillus subtilis* (ATCC 6633), *Staphylococcus aureus* (ATCC 6538)*, Escherichia coli* (ATCC 8739*) and *Pseudomonas aeruginosa* (ATCC 9022), were purchased from the microbial type culture collection, Institute of Microbial Technology, Chandigarh, India. The petri dishes measured around 32 cm diameter and 2 cm thickness were selected. All other reagents used are of analytical grade with the high purity. The solutions were prepared using deionized water.

Chemical synthesis of CeO₂-NPs

Analytical-grade cerium chlorides (CeCl₃) were used as received without any further purification. CeO₂-NPs were prepared by sol–gel methods [11]. Briefly, 3.72 g cerium chloride salt was prepared in 10 ml deionized water and then ammonia solution was added dropwise after 10 min to the above solution till its pH reaches 10. The stirring was continued for another 2 h, until the complete precipitation was acquired. The precipitate were filtered, washed and dried overnight. Then, the obtained hydroxide powder was calcinated in a muffle furnace at 400 °C for 2 h. The final product was identified as CeO₂-NPs and subjected for further characterization.

Biosynthesis of CeO$_2$-NPs

The 10 g of *S. nigrum* leaf was finely cut and stirred with 100 ml of deionized water and boiled at 80 °C. The leaf extract was filter used Whatman No. 1. It was preserved in 100-ml Erlenmeyer flask at room temperature for further usage. Thereafter, cerium chloride salt 3.72 g was dissolved in deionized water (10 ml) with constant stirring at room temperature. For 0.5:1 *v/v* ratio, 5 ml of leaf extract was added to the 10 ml of solution containing 3.72 g of CeCl$_3$. The mixture was stirred at a room temperature of 85 °C for 4 h. The observed yellowish brown colour indicates the formation of CeO$_2$-NPs. Similarly for the 1:1, 1.5:1 and 2:1 *v/v* ratio, the leaf extract of 10, 15 and 20 ml is added to the 10 ml of CeCl$_3$ solution. Further, the precipitate was dried at 400 °C for 4 h and the obtained powder was subjected for further characterization. In the figures and tables, the biosynthesized (0.5:1, 1:1, 1.5:1 and 2:1 *v/v*) CeO$_2$-NPs represent that the leaf extract to CeCl$_3$ solution is taken in the ratio of 0.5:1, 1:1, 1.5:1 and 2:1 *v/v*, respectively.

Characterization of CeO$_2$-NPs

The synthesized CeO$_2$-NPs samples were subjected to UV–visible spectroscopy (Shimadzu UV-1650) to study the optical response and to calculate the band gap. The optical band gap energy of the nanoparticles is calculated based on the absorption spectra of the nanoparticles using the Tauc relation:

$$\alpha h\upsilon = A\left(h\upsilon - Eg\right)^{1/2} \tag{1}$$

where α is the optical absorption coefficient, $h\upsilon$ is the photon energy, E_g is the direct band gap and A is an energy-independent constant.

The average crystallite size (D) of the synthesized CeO$_2$-NPs is calculated by using Debye–Scherrer's equation:

$$D = {0.9\lambda}/{\beta\cos\theta} \tag{2}$$

The lattice constant (a), dislocation density (δ) and microstrain (ε) are calculated using the following equation:

$$d = \frac{a}{\sqrt{h^2 + k^2 + l^2}} \tag{3}$$

$$\varepsilon = \frac{\beta\cos\theta}{4} \tag{4}$$

$$\delta = \frac{1}{D^2}\text{lines}/\text{m}^2 \tag{5}$$

where D is the crystallite size, k is a shape factor ($k=0.9$ in this work), θ is Bragg angle, the wavelength of incident X-rays $\lambda=1.5406$ Å, β is the full-width at half-maximum (FWHM) and (hkl) are the Miller indices.

The effective CeO$_2$-NPs surface charges (zeta potential) were analysed, and the average particle size and size distribution of synthesized CeO$_2$-NPs were observed by using the dynamic light scattering (DLS) technique using (Malvern Mansettings Nano).

The transmission electron microscopy (TEM-PHILIPS TECNAI G2 FEI 12) was carried out to confirm the particle size, shape and interplanar spacing of CeO$_2$-NPs.

The FT-IR spectra were recorded with an FT-IR (2000) PerkinElmer using KBr plate at room temperature in the range of 4000–400 cm^{-1} with a scanning rate of 4 cm^{-1}/min to identify the presence of functional groups of leaf extract and CeO$_2$-NPs.

The photoluminescence (PL) behaviour was premeditated at room temperature by Fluorolog-3 HORIBA Jobin–Yvon with an excitation wavelength of 325 nm.

Photocatalytic activity

By performing the methylene blue dye degradation reactions under stimulated sunlight irradiation, the photocatalytic activity of Chem CeO$_2$-NPs and biosynthesized CeO$_2$-NPs was analysed. In this experiment, 100 ml of 5×10^{-3} M aqueous methylene blue solution and 0.2 g of fine powder catalyst (from Chem CeO$_2$-NPs and biosynthesized (1.5:1 *v/v*) CeO$_2$-NPs) were taken. The measurement period of photocatalytic was ranging from 0 to 50 min. In order to achieve the adsorption the adsorption–desorption equilibrium between the dye and nanoparticles, the suspension was allowed for stirring in the dark for 10 min. Subsequently, the suspension was placed under sunlight radiation and took the reading after every 10 min up to 50 min and the colour of the suspension shifted from the blue to colourless. The residual solution was analysed using UV–Vis (1650 PC Shimadzu) spectrophotometer.

The percentage of methylene blue absorbed on the catalyst surface was calculated the following relation [23]:

$$\text{Degradation } (\%) = \frac{C_0 - C_t}{C_0} \times 100\% \tag{6}$$

where C_0 represents the initial absorption and C_t represents the absorption after various time intervals.

In vitro antioxidant activity

DPPH radical scavenging assay

S. nigrum leaf extract, Chem CeO$_2$-NPs and biosynthesized (1.5:1 *v/v*) CeO$_2$-NPs were tested for the scavenging effect on DPPH (1′1-diphenyl-2-picryl hydroxyl)

radical methods, as reported in Das et al. [24]. The different concentrations 15, 30, 60, 125, 250 and 500 µg/ml of test sample solution were added, in equal volume to 0.1 mM methanolic DPPH solution. The reaction mixture was incubated at room temperature for 60 min. The optical intensity of the peak 517 nm was measured for the mixture, which gives the antioxidant activity. Ascorbic acid was used as a standard to calibrate the resultant activity. Using the following equation, the percentage DPPH radical scavenging activity (RSA) of the sample was calculated:

$$\% \text{ DPPH radical scavenging}$$
$$= \left(\frac{\text{Absorbance of control} - \text{absorbance of test sample}}{\text{Absorbance of control}} \right) \times 100 \quad (7)$$

Hydroxyl radical scavenging assay

Hydroxyl radical scavenging activities of aqueous leaf extract of *S. nigrum*, Chem CeO_2-NPs and biosynthesized (1.5:1 *v/v*) CeO_2-NPs were measured using the deoxyribose method [25]. The reaction mixture contained 500 ml of 2-deoxyribose (2.8 mM), and to this mixture potassium phosphate buffer solution (50 mM, pH 7.5), 200 ml of premixed ferric chloride (100 mM) and ethylene diamine tetraacetic acid (100 mM) solution (1:1 *v/v*) and 100 ml of H_2O_2 (200 mM), either with or without the samples (100 ml) in different concentrations 15, 30, 60, 125, 250 and 500 µg/ml, were added. Then, it was triggered by adding 100 ml of 300 mM ascorbate. It was incubated for 1 h at 37 °C. A solution of thiobarbituric acid (TBA) in 1 ml of 50 mM sodium hydroxide (NaOH) and 1 ml of trichloroacetic acid (TCA) was added. The mixture was heated at 100 °C for 15 min; for colour development the intensity of the green colour formed was measured at 531 nm with a spectrophotometer. Ascorbic acid was used as a standard to calibrate the resultant activity. The scavenging percentage was calculated according to the following formula:

$$\% \text{ Hydroxyl radical scavenging} = [\text{Absorbance of the control}$$
$$- (\text{Absorbance after adding sample} - \text{Absorbance sample with deoxyribose})] \quad (8)$$
$$\times 100/\text{Absorbance of the control}$$

Antibacterial analysis

The antibacterial properties of aqueous leaf extract of *S. nigrum*, Chem CeO_2-NPs and biosynthesized (1.5:1 *v/v*) CeO_2-NPs were investigated by Kirby Bauer disc diffusion method [26]. The technique was studied by using clinically isolated bacterial culture such as Gram-positive bacteria (*Bacillus subtilis* and *Staphylococcus aureus*)

and Gram-negative bacteria (*Escherichia coli* and *Pseudomonas aeruginosa*). The bacterial suspension was swabbed on the molten nutrient agar, and it was poured into the plates using sterile cotton swabs sterile wells and prepared with the assist of a sterilized stainless steel sterile cork borers. The plates were incubated at 35 °C for 48 h. The 50 μl and 100 μl of the *S. nigrum* leaf extract, Chem CeO$_2$-NPs and bio-synthesized (1.5:1 *v/v*) CeO$_2$-NPs were added to the 25 micrograms of ciprofloxacin which was used as positive control. The diameter of the zone of inhibition (mm) was measured [27] and is given in the table.

Statistical analysis

Data were statistically analysed by sigma plot 12.5 program; mean value for three replications and standard error (SE) were calculated.

Results and discussion

UV–visible analysis

The optical absorption measurement is carried out for Chem CeO$_2$-NPs and biosynthesized CeO$_2$-NPs (Fig. 1). The absorption peaks are observed at 326, 345, 347, 355 and 351 nm for Chem CeO$_2$-NPs and biosynthesized (0.5:1, 1:1, 1.5:1 and 2:1 *v/v*) CeO$_2$-NPs, respectively, and all these values are red-shifted when compared with the absorption edge (326 nm) of Chem CeO$_2$-NPs. Similar absorption peak
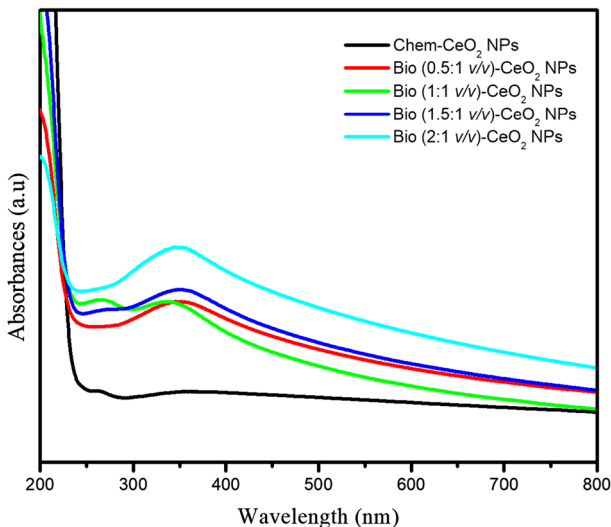
**Fig. 1** UV–visible spectra of Chem CeO$_2$-NPs and biosynthesized (0.5:1, 1:1, 1.5:1 and 2:1 *v/v*) CeO$_2$-NPs

obtained for biosynthesized CeO_2-NPs at 315 nm was reported by Maqbool et al. [28]. The *S. nigrum* leaf extract consists of phytochemicals which act as a capping and reducing agent and is also the reason for the shift of absorption peak in the UV region. As the leaf extract was increased, the reduction rate was also increased. For *S. nigrum* leaf extract of 1.5:1 *v/v*, a fast reduction was observed as indicated by yellowish to purple brown colour of the solution. Due to the deficiency of bio-molecules, the lower percentage of leaf extract (0.5:1 *v/v*) does not protect them from aggregation. The increased concentration of 1.5:1 *v/v* of leaf extract enhanced with phytochemicals content reduces the precursor quickly and formation of nano-particles increases. It has been suggested that the absorption position depends on the particle size and shape of CeO_2-NPs. The UV–visible absorption ability of CeO_2-NPs is associated with band gap energy, and this differs with different shapes of CeO_2-NPs. The band gap of synthesized CeO_2-NPs is calculated by Tauc's plot [29].

The band gap energy of Chem CeO_2-NPs and biosynthesized CeO_2-NPs values is found to be 3.80, 3.59, 3.57, 3.49 and 3.53 eV, respectively (Fig. 2). It can be seen that the band gaps of the biosynthesized CeO_2-NPs were lower than that the Chem CeO_2-NPs. The band gap energy decreases as the concentration of *S. nigrum* leaf extract increases from 0.5:1 to 1.5:1 *v/v*. The strong interaction between CeO_2 and phytochemicals (flavonoids and proteins) of *S. nigrum* leaf extract enables a faster electron recombination process; due to this, a decrease in band gap was observed for biosynthesized (1.5:1 *v/v*) CeO_2-NPs. However, the band gap energy further slightly increases in the biosynthesized (2:1 *v/v*) CeO_2-NPs due to attribute to the quantum confinement effect [10]. The observed band gap value 3.49 eV for biosynthesized (1.5:1 *v/v*) of CeO_2-NPs is suitable for exciting electron from valance to conduction band in the formation of excitation, which actively involves photocatalytic and anti-bacterial activity.
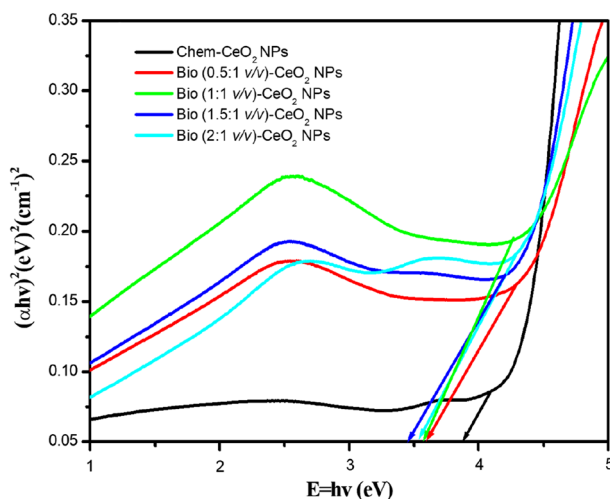
Fig. 2 Band gap energy Chem CeO_2-NPs and biosynthesized (0.5:1, 1:1, 1.5:1 and 2:1 *v/v*) CeO_2-NP
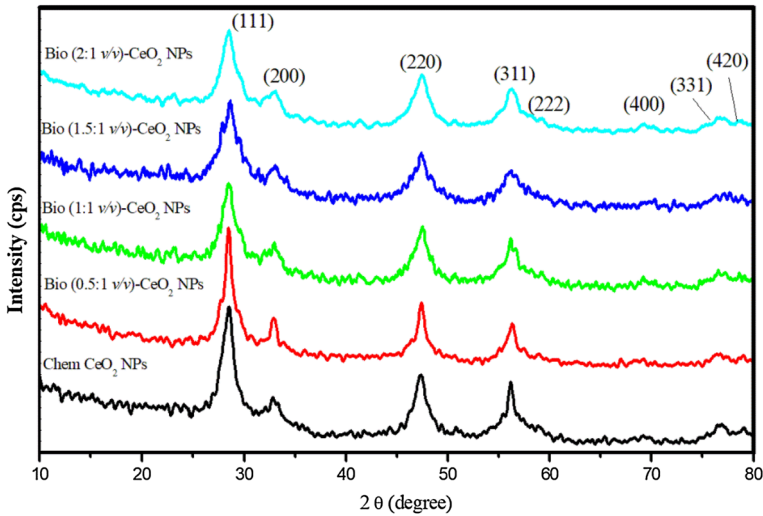
Fig. 3 X-ray diffraction pattern of Chem CeO₂-NPs and biosynthesized (0.5:1, 1:1, 1.5:1 and 2:1 *v/v*) CeO₂-NPs

Table 1 Structural parameters of Chem CeO₂-NPs and biosynthesized (0.5:1, 1:1, 1.5:1 and 2:1 *v/v*) CeO₂-NPs

Sample name	Lattice parameter (Å)	Dislocation density(δ) $\times10^{15}$ (l/m^2)	Microstrain (ε) $\times10^{-3}$	Crystallite size (nm)
Chem CeO₂ NPs	5.410	4.36	2.63	15.14
Bio (0.5:1 *v/v*) CeO₂-NPs	5.415	4.72	2.84	14.55
Bio (1:1 *v/v*) CeO₂-NPs	5.435	7.85	3.65	11.28
Bio (1.5:1 *v/v*) CeO₂-NPs	5.450	8.29	2.91	10.08
Bio (2:1 *v/v*) CeO₂-NPs	5.428	5.42	3.47	11.50

Structural analysis

The X-ray diffraction patterns of Chem CeO₂-NPs and biosynthesized CeO₂-NPs with different percentage of *S. nigrum* leaf extract are shown in Fig. 3. The sharp high intense diffraction peaks reveal the crystal structure and purity. The majority of the perceptible Bragg's speaks with Miller indices (111), (200), (220), (222), (400), (331), (420) and (422) can be recorded to the cubic structure of CeO₂-NPs (JCPDS NO: 043-1002) [30]. The peak intensity decreases with an increase in *S. nigrum* leaf extract percentage [31]. The decrease in peak intensity is due to an increase in full-width at half-maximum (FWHM) of prepared samples. The Scherrer's formula was used to determine the mean crystallite size of samples.

From Table 1, the crystal size for Chem CeO₂-NPs is 15.14 nm. The crystal size decreases for biosynthesized CeO₂-NPs, with increasing percentage of *S. nigrum* leaf extract and is found to be 10.08 nm (up to 1.5:1 *v/v*). The minimum crystallite

size is observed for biosynthesized (1.5:1 *v/v*) CeO$_2$-NPs due to quantum confinement effect. The crystallite size increased to 11.50 nm at higher percentage of (2:1 *v/v*) *S. nigrum* leaf extract. This may be due to a decrease in grain boundaries because of increasing crystallite with a lower number of lattice imperfections.

The lattice constant, microstrain and dislocation density of Chem CeO$_2$-NPs and biosynthesized CeO$_2$-NPs were evaluated by using the respective formula [32]. The lattice constant (Å), microstrain and dislocation density (lines/m^2) values are reported in Table 1. From the table, it can be observed that the lattice constant increases (5.410–5.450 Å) with an increase in *S. nigrum* leaf extract percentage up to 1.5:1 *v/v*. The slow change in lattice constant for the biosynthesized CeO$_2$-NPs over the bulk clearly indicates that the particles are strained which may be due to the nature and percentage (leaf extract) of the native imperfections changing. However, both microstrain and dislocation density increased with increasing percentage of *S. nigrum* leaf extract. The present work shows that biosynthesized (1.5:1 *v/v*) CeO$_2$-NPs small crystallite size (10.08 nm) will help greatly to improve the photocatalytic and antibacterial activity.

DLS and Zeta potential analysis

The particle size distribution of the sample is analysed by performing DLS technique, which is in the form of hydrodynamic radius considering each particle as a separate sphere in Brownian movement [33]. The DLS is mainly used to determine particle size and the shell thickness of a capping or stabilizing agent which develops the metallic nanoparticles [34]. A narrow range of particle size distribution can be observed, and the average particle size is calculated based on Fig. 4a–b for Chem CeO$_2$-NPs and biosynthesized (1.5:1 *v/v*) CeO$_2$-NPs 97 and 45 nm, respectively.
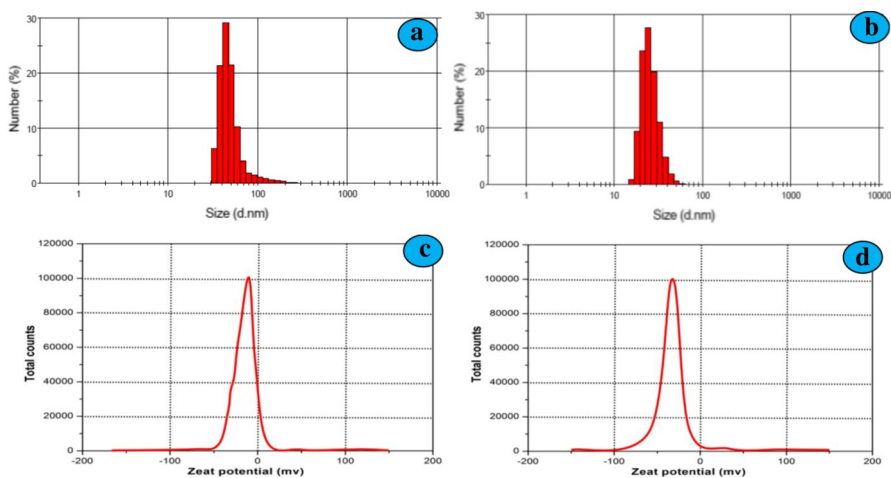
Fig. 4 a–b Dynamic light scattering (DLS) pattern; **c–d** zeta potential distribution of Chem CeO$_2$-NPs and biosynthesized (1.5:1 *v/v*) CeO$_2$-NPs

Zeta potential (ZP) values expose details regarding the surface area charge and also the stability of samples. Figure 4c–d shows the Chem CeO$_2$-NPs and biosynthesized (1.5:1 v/v) CeO$_2$-NPs have average ZP values of − 15.12 and − 25.83 mV, respectively. The ZP values of − 25.83 mV clearly indicate that the biosynthesized CeO$_2$-NPs have good stability. The high negative values of zeta potential confirm that the capping particles present on the surface of CeO$_2$-NPs are mainly comprised with negatively charged groups which have moderate stability of the nanoparticles. The proteins in the *S. nigrum* leaf extract are responsible for reducing metal ions. They are efficient in stabilizing the synthesizing nanoparticles.

HR-TEM analysis

High-resolution transmission electron microscopy (HR-TEM) vividly demonstrates the morphology and particles size of the synthesized CeO$_2$-NPs. Typical TEM images obtained for Chem CeO$_2$-NPs and biosynthesized CeO$_2$-NPs using *S. nigrum* leaf extract (1.5:1 v/v) are shown in Figs. 5 and 6. The morphology of synthesized
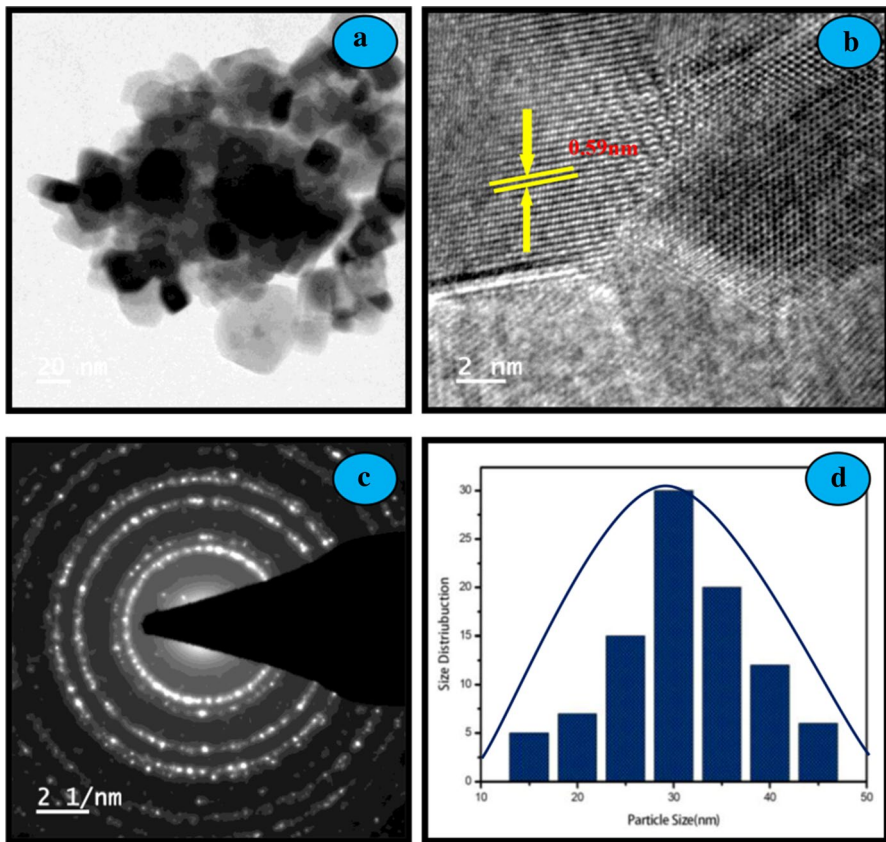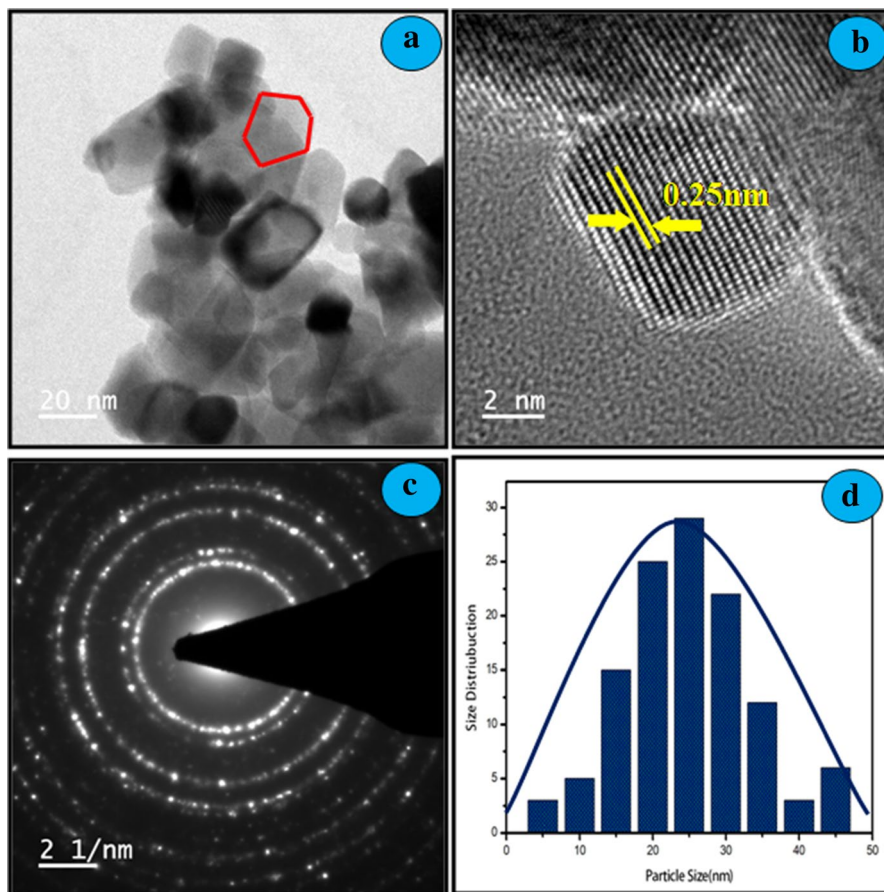

Fig. 5 **a** HR-TEM image; **b** lattice fringe; **c** SAED pattern; **d** particle size of Chem CeO$_2$-NPs

Fig. 6 **a** HR-TEM image; **b** lattice fringe; **c** SAED pattern; **d** particle size of biosynthesized (1.5:1 *v/v*) CeO_2-NPs

CeO_2-NPs is almost cubic nanocrystals. The histogram that shows particle size distribution is given in Figs. 5 and 6. The width of the histogram is narrower, and the average particle size is 32 and 20 nm for Chem CeO_2-NPs and biosynthesized CeO_2-NPs, respectively. The observed particle size in HR-TEM is lower than the value determined from the particle size analyser (DLS). In fact, DLS measures the hydrodynamic diameter of the synthesized CeO_2-NPs, whereas the diameter observed by HR-TEM indicates that of dried CeO_2-NPs. The selected area electron diffraction (SAED) pattern with bright circular spots corresponding to (1 1 1), (2 0 0), (2 2 0), (3 1 1), (2 2 2), (4 0 0), (3 3 1) and (4 2 0) planes the crystalline nature of the biosynthesized CeO_2-NPs confirm. No other rings are seen in the SAED pattern from its crystalline impurities [35]. The particle size is in very close agreement with the average particle size from XRD pattern [36].
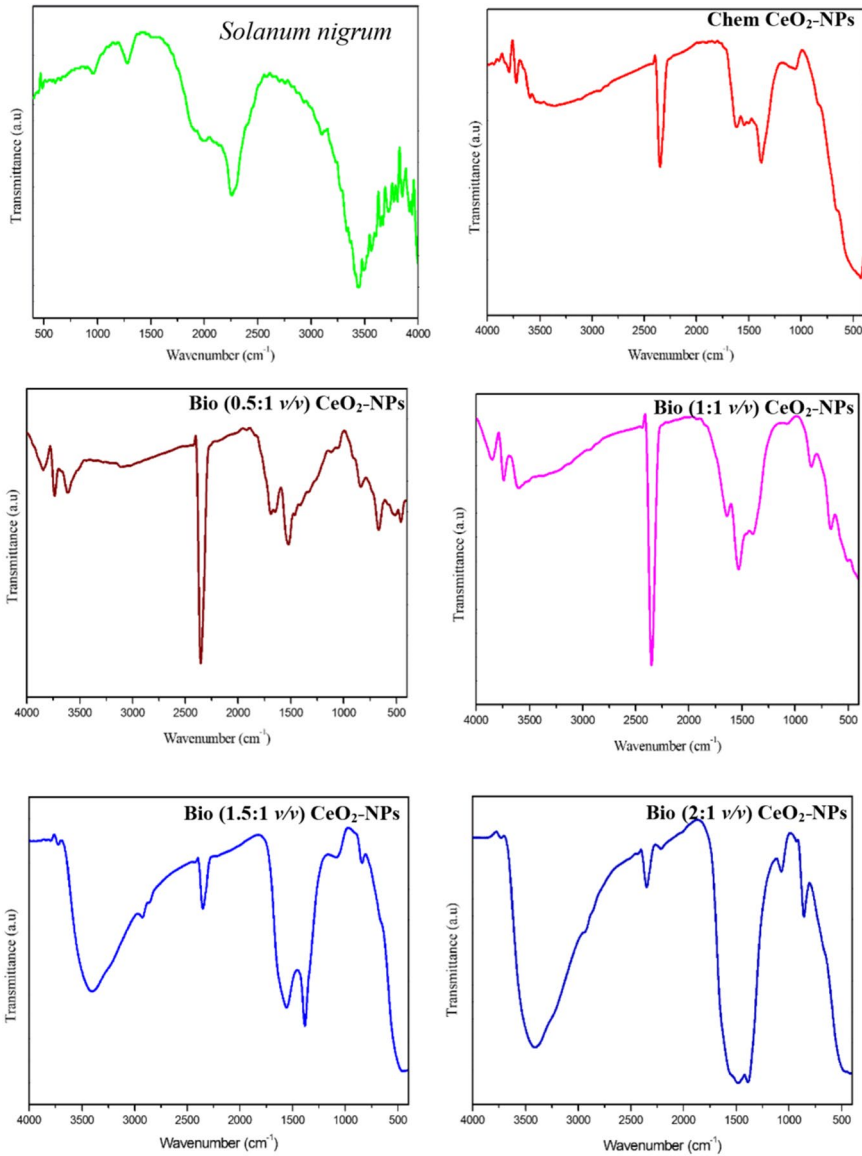
Fig. 7 FT-IR spectrum of *S. nigrum* leaf extract, Chem CeO$_2$-NPs and biosynthesized (0.5:1, 1:1, 1.5:1 and 2:1 *v/v*) CeO$_2$-NPs

FT-IR analysis

FT-IR spectroscopy helps to know the biomolecules attached to the surface of CeO$_2$-NPs from the leaf extract. FT-IR spectra of dried leaf extract of *S. nigrum*, Chem CeO$_2$-NPs and biosynthesized CeO$_2$-NPs are shown in Fig. 7. The peaks and

Table 2 Functional group and commonly assigned component of *S. nigrum* leaf extract, Chem CeO$_2$-NPs and biosynthesized (0.5:1, 1:1, 1.5:1 and 2:1 *v/v*) CeO$_2$-NPs

Wavenumber (cm^{-1})		Bio CeO$_2$-NPs				Functional group and commonly assigned component
S. nigrum leaf extract	Chem CeO$_2$-NPs	0.5:1 *v/v*	1:1 *v/v*	1.5:1 *v/v*	2:1 *v/v*	
–	3721.61	–	3735.62	3735.92	–	Water O–H Stretch
3453.29	–	3392.10	–	–	3467.14	Free O–H bonding
3105.32	–	2923.38	–	–	–	Symmetric and asymmetric stretching vibration
2263.63	2330.53	2357.61	2352.94	2352.35	2383.37	C–H stretching
2013.40	–	–	–	–	–	C–C=–C–C=–CH
–	1606.01	–	–	1686.52	–	Amide II band or N–H primary amines
–	–	1554.85	1525.51	1517.93	1474.35	CH$_2$ bond
1997.48	–	–	–	–	–	No conjugation
1284.63	1371.28	1369.02	1361.25	1375.20	1371.23	CH$_3$ mode of organic moieties
961.12	–	844.63	844.63	844.63	844.63	C–O stretching mode of vibrations

its assignments are shown in Table 2. The *S. nigrum* leaf extract showed absorption peaks at 3453.29, 3105.32, 2263.63, 2013.40, 1997.63, 1284.63 and 961.12 cm^{-1}. The peak at 3453.29 cm^{-1} corresponds to N–H stretching and bending vibrations. The peak at 3105.32 cm^{-1} can also be related to O–H stretching vibration of alcohols and phenols. The O–H and N–H are the main functional groups present in the proteins, phenolic compounds, vitamins, flavonoids, alkaloids, terpenes, tannins and saponin [22].

No additional peaks are observed, and some of the peak positions in biosynthesized CeO$_2$-NPs are slightly shifted towards higher wavenumbers when compared to that of Chem CeO$_2$-NPs. The shift is due to an interaction of *S. nigrum* leaf extract with CeO$_2$-NPs and solvent during biosynthesis. The FT-IR peaks of biosynthesized CeO$_2$-NPs at 3392 cm^{-1} (free O–H bonding) [37], 2923 cm^{-1} (symmetric and asymmetric stretching vibration) [38], 2357 cm^{-1} (C–H stretching), 1686 cm^{-1} (amide II band or N–H primary amines), 1525 cm^{-1} (CH$_2$ bond), 1380 cm^{-1} (CH$_3$ is due groups), 1056 cm^{-1} (vinyl group), 841 cm^{-1} (C–O stretching mode of vibrations), similar to the FT-IR bands of CeO$_2$-NPs are reported in the literature [39]. The phytochemical analysis of the dried leaf extract of *S. nigrum* has been reported to show the presence of proteins, phenolic compounds, vitamins, flavonoids, alkaloids, terpenes, tannins and saponin [40]. The flavonoids present in the leaf extract are powerful reducing agents, which may be responsible for the reduction of cerium chloride heptahydrate salt. These flavonoids as well act as a surfactant and attach to the surface of CeO$_2$-NPs, and it stabilizes CeO$_2$-NPs through electrostatic stabilization. Consequently, it is discovered that *S. nigrum* leaf extract has the ability to perform dual function of reduction and stabilization of CeO$_2$-NPs.
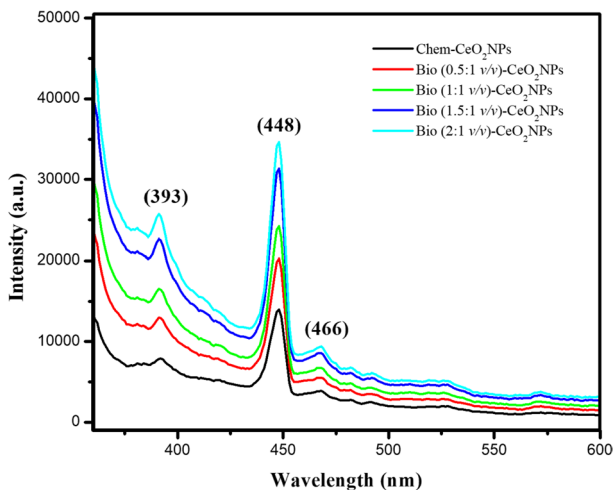
Fig. 8 Photoluminescence spectra of Chem CeO$_2$-NPs and biosynthesized (0.5:1, 1:1, 1.5:1 and 2:1 *v/v*) CeO$_2$-NPs

Photoluminescence analysis

Photoluminescence spectroscopy (PL) is normally used to explore the efficiency of charge carrier migration and transfer and also to understand the fate of the electron hole pairs in semiconductors [41]. In the present work, PL spectrum is used to get important information about the surface defect, oxygen vacancies and surface states which can strangle the effect of the photocatalytic reaction. Figure 8 shows room temperature PL spectra of Chem CeO_2-NPs and biosynthesized CeO_2-NPs. Both the samples exhibit similar peaks position but differ in intensities. PL intensity increases with increasing *S. nigrum* of leaf extract percentage. The emission spectra of synthesized CeO_2-NPs contain three peaks 393, 448 and 466 nm representing for near-band-edge (NBE) emissions: a violet emission and two blue emissions, respectively. The Chem CeO_2-NPs PL emission peak located at 393 nm (NBE) is attributed to excitonic recombination. It is due to the 5d–4f transitions of Ce^{3+} between the ^2D ($5d_1$) ground state and the $^2F_{5/2}$ ($4f_1$) state [42]. The emission peak appeared at 448 and 466 nm is associated with oxygen vacancies [43]. Biosynthesized CeO_2-NPs luminescence bands at 445 and 466 nm are blue-shifted compared to Chem CeO_2-NPs. Due to transition of oxygen vacancy and interstitial oxygen, the blue emission peak is located at 445 nm. Hence, the defects and the oxygen vacancies present in the biosynthesized CeO_2-NPs help to fuse the photo-induced electron easily to form excitons. This demonstrates the increase in PL intensity. The enhanced PL reveals intensity of the good crystalline nature of biosynthesized CeO_2-NPs and exhibits desirable properties for catalysis application.

Photocatalytic activity

Among many rare earth elements, CeO_2-NPs are environmental friendly due to their photocatalytic application, from ecological point of view. Industrial wastes contain different types of toxic chemical and organic dyes, which are discharged to water bodies. It produces heavy impact on the environment. All the dyeing agents are stable organic compounds. Methylene blue dye shows different colours in both oxidized and reduced forms so it is selected for the study.

The photocatalytic activity is carried out for Chem CeO_2-NPs and biosynthesized (1.5:1 *v/v*) CeO_2-NPs in order to study the degradation of aqueous solution of methylene blue dye in open air sunlight. The catalytic degradation of dye is shown in Fig. 9a, c. The UV–Vis spectra are recorded from 200 to 800 nm for various time intervals 0, 10, 20, 30, 40 and 50 min. The UV absorption peaks at 292 and 665 nm indicate if it is the methylene blue dye, the dark blue colour of the dye is reduced into colourless form due to the electron transition. The bands observed at 665 nm indicate that 78.14 and 94.58% of dye are degraded at exactly 50 min due to the catalytic efficiency Chem CeO_2-NPs and biosynthesized CeO_2-NPs, respectively (Table 3). An improved reduction rate is observed when the catalyst is added. This is on the transitional redox potential incentive between the benefactor and acceptor through the electron move process. Biosynthesized CeO_2-NPs perform as efficient redox catalyst which has the electron relay effect. It is well known that the
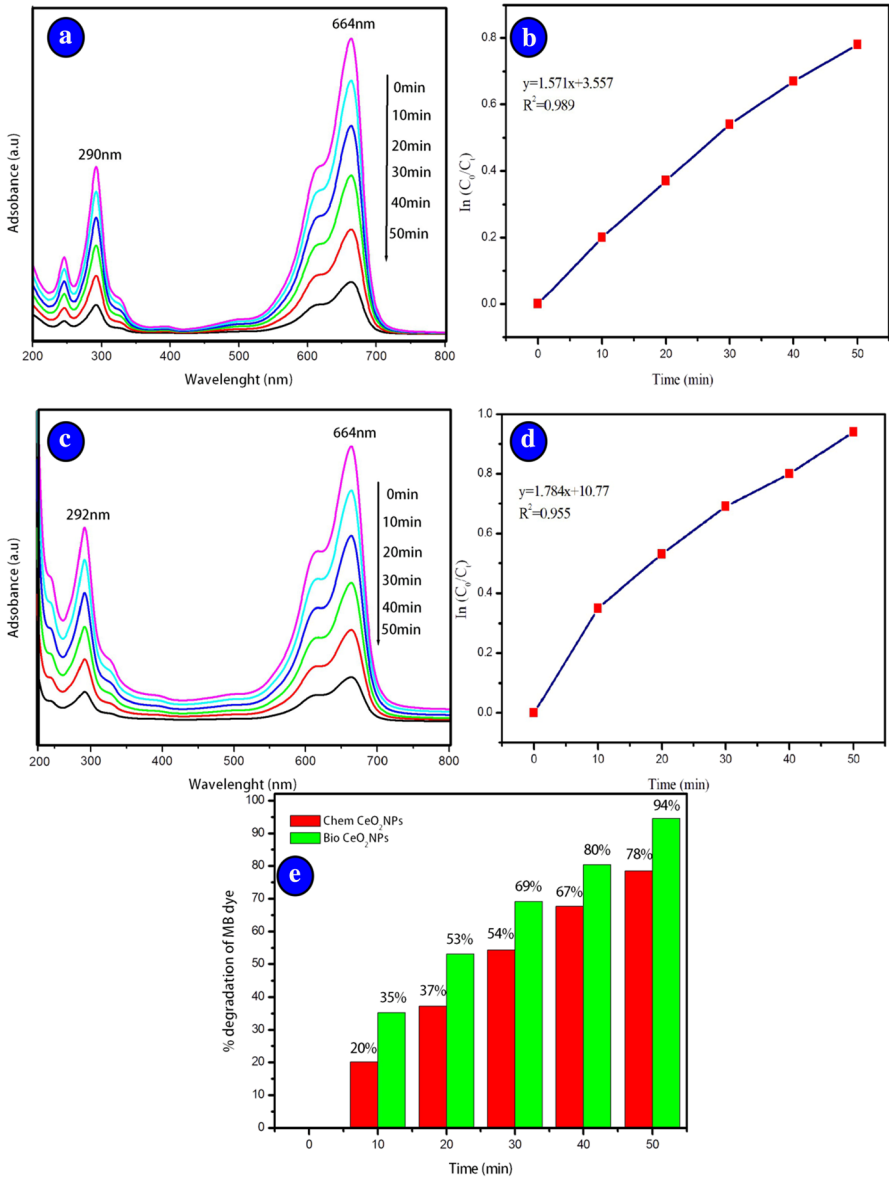
Fig. 9 **a, c** UV–Vis absorption spectra of methylene blue dye with respect to irradiation time versus **b, d** rate constant (K) and regression (R^2); **e** % degradation of methylene blue dye compared to the Chem CeO$_2$-NPs and biosynthesized (1.5:1 v/v) CeO$_2$-NPs

size of metal nanoparticles plays a significant role in catalytic reduction, whereas an increase in the number of low coordinated cerium atoms is occurred with a decrease in the size of biosynthesized CeO$_2$-NPs, which encourages the adsorption of the reactants on the catalyst surface and facilitates the degradation. Hence, an increase

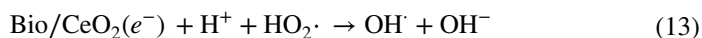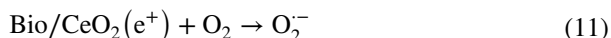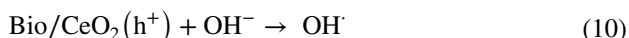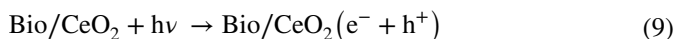**Table 3** Effect of methylene blue dye degradation by Chem CeO_2-NPs and biosynthesized (1.5:1 *v/v*) CeO_2-NPs

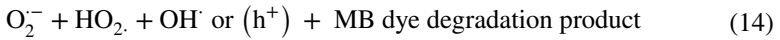| Time (min)	% degradation of methylene blue dye	
	Chem CeO_2-NPs	Bio CeO_2-NPs
0	0	0
10	20.13	35.15
20	37.19	53.10
30	54.23	69.12
40	67.03	80.42
50	78.43	94.58

in the surface areas of the particles will significantly enhance the effectiveness of the catalyst.

Mechanism of photocatalytic activity

The different amounts of oxygen vacancies show the distinction of photocatalytic performance. The quantity of oxygen opening demonstrates the division of electron gap sets. They also suggest that much more oxygen vacancies would allow fast electron–hole recombination, thereby decreasing the photocatalytic activity for Chem CeO_2-NPs [44]. According to Malleshappa et al. [45], the differences in photocatalytic activity were highly related to the concentration defects on the surface of the nanoparticles. They also had stated that surface defects were increased with the decrease in particles size and hence the charge carrier recombination rate was increased which results in the raise photocatalytic activity. In the present study, biosynthesized CeO_2-NPs having smallest particle sizes show high photocatalytic activity, which is attributed to the high abilities of separating the photogenerated charge carriers, large specific surface area and enhanced light absorption.

Based on the above, the possible mechanism for the methylene blue dye photodegradation over biosynthesized CeO_2-NPs irradiated by sunlight is as follows:

$$Bio/CeO_2 + h\nu \rightarrow Bio/CeO_2\left(e^- + h^+\right) \tag{9}$$

$$Bio/CeO_2\left(h^+\right) + OH^- \rightarrow OH^{\cdot} \tag{10}$$

$$Bio/CeO_2\left(e^+\right) + O_2 \rightarrow O_2^{\cdot-} \tag{11}$$

$$O_2^{\cdot-} + H+ \rightarrow HO^{2\cdot} \tag{12}$$

$$Bio/CeO_2(e^-) + H^+ + HO_2\cdot \rightarrow OH^{\cdot} + OH^- \tag{13}$$

$$O_2^- + HO_{2.} + OH^. \text{ or } (h^+) + MB \text{ dye degradation product} \qquad (14)$$

From the above reaction steps, when the biosynthesized CeO$_2$-NPs are irradiated by sunlight, electron (e$^-$) in the valence band (VB) can be excited to the conduction band (CB) and, simultaneously, the same numbers of holes (h$^+$) are generated in the VB. To deliver a solid oxidant OH$^-$ radical species, the photoinitiated openings legitimately respond with methylene blue colour or connect with surface bound H$_2$O or OH$^-$. It is suggested that the electron formed can react with the adsorbed molecular oxygen to yield O$_2^-$. This combines with H$^+$ to produce HO·$_2$, which reacts with the trapped electron to generate OH$^.$ radical. Thus, the produced reactive species such as OH$^.$, HO$_2^.$ and O$_2^-$ could degrade the methylene blue dye.

Kinetic studies

The pseudo-first-order kinetics of the degradation of organic dyes by photocatalysts is [26].

$$In \left(C_0/C_t \right) = -kt \qquad (15)$$

where k is the apparent reaction rate constant, C_0 is the initial concentration of aqueous methylene blue, t is the reaction time and C is the concentration of aqueous methylene blue dye at the reaction time t.

The kinetics of photodegradation of methylene blue by Chem CeO$_2$-NPs and biosynthesized CeO$_2$-NPs are studied, and results are shown in Fig. 9b, d. The rate constant (K) for methylene blue dye degradation by synthesized CeO$_2$-NPs is determined by the pseudo-first-order rate equation. The plot of In (C_0/C_t) as a function of irradiation time gives the rate constant values 1.571 and 1.784 min^{-1}; moreover, the fitting correlation coefficient (R^2) is also determined to be 0.989 and 0.955 for Chem CeO$_2$-NPs and biosynthesized CeO$_2$-NPs. Finally, it is concluded that C_0/C_t is decreased with increasing time and vice versa. The percentage of dye degradation is increased with the increase in time (Fig. 9e). According to the result, the biosynthesized CeO$_2$-NPs showed better photocatalytic activity on methylene blue dye compared with Chem CeO$_2$-NPs as well as other literature values [46].

In vitro antioxidant activity

DPPH radical scavenging assay

DPPH is stable nitrogen-centred free radical commonly used for resting radical scavenging activity for the compound or plants extract. The stable DPPH assay is reduced by accepting electron or hydrogen [47]. DPPH radical scavenging activity of *S. nigrum* leaf extract, Chem CeO$_2$-NPs and biosynthesized (1.5:1 *v/v*) CeO$_2$-NPs is measured at different concentrations of 15, 30, 60, 125, 250 and 500 μg/ml for
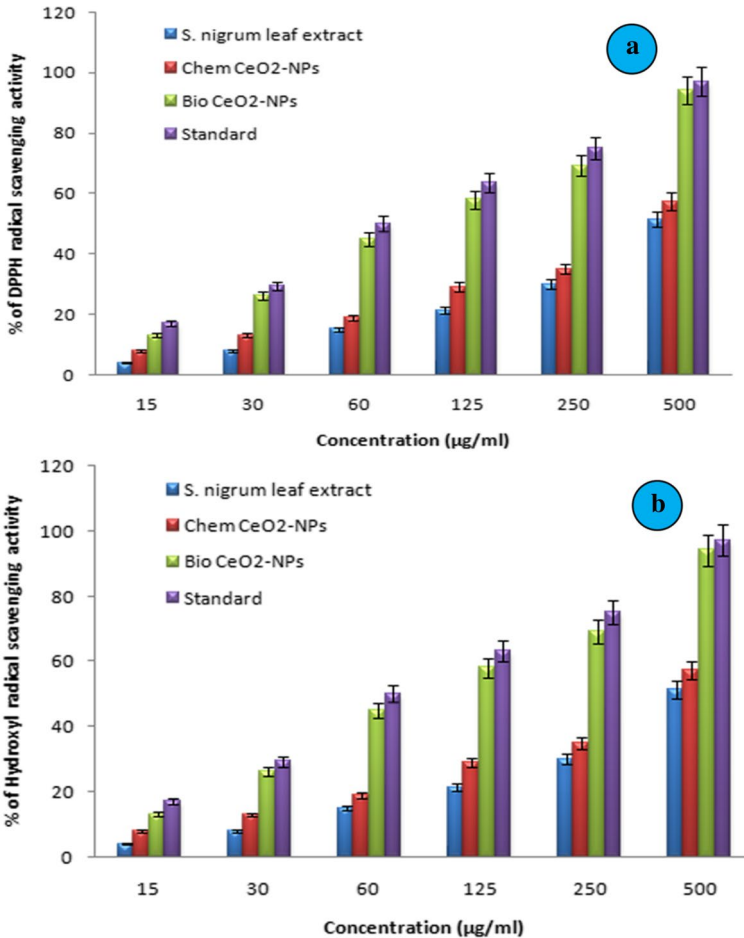
Fig. 10 **a** DPPH free radical; **b** hydroxyl radical scavenging assay of *S. nigrum* leaf extract, Chem CeO_2-NPs and biosynthesized (1.5:1 *v/v*) CeO_2-NPs

used ascorbic acid in standard. The reducing activity of *S. nigrum* leaf extract, Chem CeO_2-NPs and biosynthesized CeO_2-NPs is quantified spectrophotometrically by changing the DPPH colour from the initial blue/purple solution to a yellow, and the DPPH activity of the *S. nigrum* leaf extract, Chem CeO_2-NPs and biosynthesized CeO_2-NPs is found to increase in a dose-dependent manner. The per cent inhibition of DPPH radical scavenging activity is presented in Fig. 10a. The calculated half maximal inhibitory concentration (IC_{50} µg/ml) values are 189 ± 12, 171 ± 19, 139 ± 45 and 124 ± 34 for *S. nigrum* leaf extract, Chem CeO_2-NPs, biosynthesized CeO_2-NPs and standard, respectively. The potency for antioxidant activity of the extract is greater when IC_{50} µg/ml values are lower. The investigation of DPPH scavenging activity observed the highest inhibition in biosynthesized CeO_2-NPs compared to the *S. nigrum* leaf and Chem CeO_2-NPs. This result is in agreement with

the study of Fatemesh et al., which had shown antioxidant activity of plants extract *Ceratonia siliqua* using biosynthesized CeO$_2$-NPs [48]. In addition, Krishanaveni et al. [49] obtained similar results by using biosynthesized CeO$_2$-NPs from *Clitoria ternatea*. The possible reason for antioxidant activity of *S. nigrum* leaf extract may be related to bioactive phytochemicals such as flavonoids, alkaloids and phenolic compounds in it; thus, reducing plants' metabolite concentration during the formation of nanoparticles may lead to a decrease in free radical scavenging activity of nanoparticles.

Hydroxyl radical scavenging assay

Hydroxyl radical can be formed by the Fenton reaction in the presence of reduced transition metals (such as, Ce^{3+}) and H$_2$O$_2$, which is known as the significant dynamic oxygen species causing lipid peroxidation and gigantic natural harm. Hydroxyl radical (OH·) is a cancer prevention agent movement due to its reactivity of the OH· which empowers it to respond with the scope of atoms found in living cells such as sugars, amino acids, lipids and nucleotides [50] and removes OH· which is very important for the protection of living systems. The OH· scavenging potential of various solvents of *S. nigrum* leaf extract, Chem CeO$_2$-NPs and biosynthesized (1.5:1 *v/v*) CeO$_2$-NPs is shown in Fig. 10b. The calculated IC$_{50}$ μg/ml values are 184 ± 13, 168 ± 24, 131 ± 21 and 119 ± 18 for *S. nigrum* leaf extract, Chem CeO$_2$-NPs, biosynthesized CeO$_2$-NPs and standard, respectively. The investigation of OH· scavenging activity observed the highest inhibition in biosynthesized CeO$_2$-NPs compared to the *S. nigrum* leaf and Chem CeO$_2$-NPs. The same kind of activities are observed when exposed to CeO$_2$-NPs which are produced from *Aspergillus niger* [51]. Cerium oxide has large surface area, and so more phytochemical compounds are adsorbed onto the active surface. Therefore, shell reaction phenomenon of the *S. nigrum* leaf extract-mediated biosynthesized CeO$_2$-NPs (due to adsorbed antioxidant moiety onto the surface) is elevated in scavenging the free radical.

Antibacterial activity

The antibacterial effect of *S. nigrum* leaf extract, Chem CeO$_2$-NPs and biosynthesized (1.5:1 *v/v*) CeO$_2$-NPs towards various pathogenic organisms such as Gram-positive bacteria (*Bacillus subtilis and Staphylococcus aureus*) and Gram-negative bacteria (*Escherichia coli and Pseudomonas aeruginosa*) is investigated, and zone of inhibition is observed for the concentration of 50 μl and 100 μl as shown in Fig. 11. The diameter of inhibition zone (mm) is given in Table 4. It is clear that the biosynthesized CeO$_2$-NPs show better antibacterial activity than Chem CeO$_2$-NPs and *S. nigrum* leaf extract. It is well known that the particle size and surface area play a key role in their interrelation with the biological cells or to produce secondary products that cause damage. CeO$_2$-NPs produce electronic effects and these effects because of their size and large surface area. These electronic impacts improve the
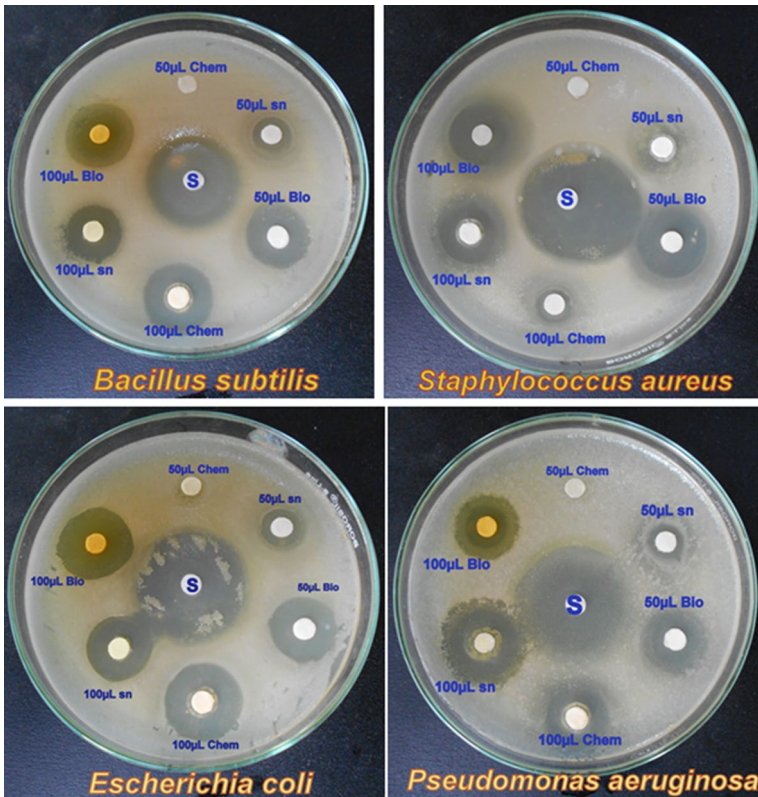
Fig. 11 Antibacterial activity of *S. nigrum* leaf extract, Chem CeO$_2$-NPs and biosynthesized (1.5:1 *v/v*) CeO$_2$-NPs

coupling quality of the nanoparticles with the microbes. Hence, the CeO$_2$-NPs can be easily attached to the cell membrane and penetrated into the bacteria [52]. It is clear that the above mechanisms confirm higher antibacterial activity of biosynthesized CeO$_2$-NPs compared to the *S. nigrum* leaf extract and Chem CeO$_2$-NPs. According to the obtained results, biosynthesized CeO$_2$-NPs exhibit effective zone of inhibition against Gram-negative bacteria compared to the Gram-positive bacteria. The cell wall between Gram-positive bacteria has one cytoplasmic membrane with a multilayer peptidoglycan, consisting of linear polysaccharide chains cross-linked by short peptides, thus forming more reside structure leading to difficult penetration of CeO$_2$-NPs compared to Gram-negative bacteria having two outer membranes with a thin peptidoglycan. In this manner, biosynthesized CeO$_2$-NPs show better antibacterial action against Gram-negative than Gram-positive microorganisms. The higher inhibitory action of biosynthesized CeO$_2$-NPs does not depend only on the size and surface area of the nanoparticles but also on capping agent (proteins) of the nanoparticles.

Table 4 Antibacterial activity of *S. nigrum* leaf extract, Chem CeO₂-NPs, biosynthesized (1.5:1 *v/v*) CeO₂-NPs and standard against human pathogenic bacteria

Bacteria	Zone of inhibition (mm)						Standard
	50 µl			100 µl			
	Chem CeO₂-NPs	*S. nigrum*	Bio CeO₂-NPs	Chem CeO₂-NPs	*S. nigrum*	Bio CeO₂-NPs	
Bacillus subtilis	0±0.2	11±0.4	19±0.1	9±0.2	14±0.1	21±0.4	25±0.6
Staphylococcus aureus	1±0.1	10±0.2	18±0.1	7±0.1	13±0.3	20±0.3	25±0.4
Escherichia coli	4±0.2	12±0.6	20±0.7	8±0.8	14±0.5	22±0.3	27±0.1
Pseudomonas aeruginosa	5±0.4	9±0.1	17±0.2	7±0.4	12±0.4	19±0.2	25±0.3

Conclusion

The CeO_2-NPs were successfully synthesized by chemical and biosynthesized using *S. nigrum* leaf extract. The *S. nigrum* leaf acts as controlled reducing and stabilizing agents in the biosynthesis of CeO_2-NPs. The optical band gap energy of Chem and biosynthesized CeO_2-NPs calculated from UV–visible absorption lies in between 3.80 and 3.49 eV. DLS studies revealed that the average size of biosynthesized CeO_2-NPs was found to be around 45 nm and zeta potential value of -25.83 mV, demonstrating the moderate stability of synthesized nanoparticles. The good polycrystalline cubic nature of synthesized CeO_2-NPs was evident from bright circular SAED pattern, which was consistent with the XRD result. FT-IR spectra obviously demonstrated the presence of bio-organic molecules of *S. nigrum* leaf extract supernatant such as carboxylate group present in proteins during the synthesis CeO_2-NPs and could act as a surfactant to attach on the surface and stabilize CeO_2-NPs throughout electrostatic stabilization. The synthesized CeO_2-NPs were found as an efficient photocatalyst for the degradation of methylene blue dye under sunlight irradiation. Among the two, the biosynthesized CeO_2-NPs photocatalyst exhibited excellent photocatalytic degradation of biosynthesized CeO_2-NPs 94.58% under the visible light irradiation. The synthesized CeO_2-NPs by this green chemistry approach had shown best antibacterial activity against Gram-negative and Gram-positive bacteria; particularly, high susceptibility was shown by *Escherichia coli.* From the results, it was clear that the biosynthesized CeO_2-NPs are one of the best candidates for environmental application and various biological- and medicinal-related applications.

Compliance with ethical standards

Conflict of interest The authors declare that they have no conflict of interest.

References

1. G. Chen, F. Zhu, X. Sun, S. Sun, R. Chen, CrystEngComm **13**, 2904 (2011)
2. J. Peng, P. Zhan, R. Deng, Y. Zhang, X. Xie, Res. Chem. Intermediat. **45**, 4637 (2019)
3. Y. Wang, T. Wu, Y. Zhou, C. Meng, W. Zhu, L. Liu, Sensors **17**, 1971 (2017)
4. K. Mondal, Invention **2**, 9 (2017)
5. V. Rai, A.K. Agnihotri, S. Khatoon, A.K.S. Rawat, S. Mehrotra, B. Environ. Contam. Tox. **74**, 464 (2005)
6. C. Korsvik, S. Patil, S. Seal, W.T. Self, Chem. Commun. **10**, 1056 (2007)
7. N. Krishna Chandar, R. Jayavel, Physica E **58**, 48 (2014)
8. S. Maensiri, S. Labuayai, P. Laokul, J. Klinkaewnarong, E. Swatsitang, J. Appl. Phys. **53**, 06JG14 (2014)
9. J. Chen, S. Patil, S. Seal, J.F. McGinnis, Nat. Nanotechnol. **1**, 142 (2006)
10. V. Ramasamy, V. Mohana, G. Suresh, I. J. M. S. C. I. **12**, 72 (2017)
11. P. Tamizhdurai, S. Sakthinathan, S.M. Chen, K. Shanthi, S. Sivasanker, P. Sangeetha, Sci. Rep. **7**, 1 (2017)
12. D. Channei, B. Inceesungvorn, N. Wetchakun, S. Phanichphant, A. Nakaruk, P. Koshy, C.C. Sorrell, Ceram. Int. **39**, 3129 (2013)
13. H.-L. Lin, C.-Y. Wu, R.-K. Chiang, J. Colloid Interface Sci. **341**, 12 (2010)
14. F. Czerwinski, J.A. Szpunar, J. Solgel Sci. Technol. **9**, 103 (1997)

15. F. Li, X. Yu, H. Pan, M. Wang, X. Xin, Solid State Sci. **2**, 767 (2000)
16. P.L. Chen, I.W. Chen, J. Am. Ceram. Soc. **76**, 1577 (1993)
17. S. Parvathy, S.R. Elavarasu, R. Meena, I. J. A. E. R. D. **4**, 1 (2017)
18. M.J. Godinho, R.F. Gonçalves, L.P.S. Santos, J.A. Varela, E. Longo, E.R. Leite, Mater. Lett. **61**, 8 (2007)
19. A. Fouda, S.E.-D. Hassan, A.M. Abdo, M.S. El-Gamal, Biol. Trace Elem. Res. (2019). https://doi.org/10.1007/s12011-019-01883-4
20. A. Arumugam, C. Karthikeyan, A.S. Haja Hameed, K. Gopinath, S. Gowri, V. Karthika, Mat. Sci. Eng. C **49**, 408 (2015)
21. K.S. Venkatesh, K. Gopinath, N.S. Palani, A. Arumugam, S.P. Jose, S.A. Bahadur, R. Ilangovan, RSC Adv. **6**, 42720 (2016)
22. K.M. Saad-Allah, M.A. Elhaak, J. Sau. Soc. Agr. Sci. **16**, 227 (2017)
23. S. Suganya, M. Jothibas, S.J. Jeyakumar, J. Mater. Sci. Mater. Electron. **30**, 7916 (2019)
24. D. Das, B.C. Nath, P. Phukon, A. kalita, S.K. Dolui, Colloids Surf. B **111**, 556 (2013)
25. R.S. Priya, D. Geetha, P.S. Ramesh, Ecotox. Environ. Safe **134**, 308 (2016)
26. A.S. Elfeky, S.S. Salem, A.S. Elzaref, M.E. Owda, H.A. Eladawy, A.M. Saeed, M.A. Awad, R.E. Abou-Zeid, A. Fouda, Carbohydr. Polym. **230**, 115711 (2020)
27. S.E.-D. Hassan, A. Fouda, A.A. Radwan, S.S. Salem, M.G. Barghoth, M.A. Awad, A.M. Abdo, M.S. El-Gamal, J. Biol. Inorg. Chem. **24**, 377 (2019)
28. Q. Maqbool, M. Nazar, S. Naz, T. Hussain, N. Jabeen, R. Kausar, S. Anwaar, F. Abbas, T. Jan, Int. J. Nanomed. **11**, 5015 (2016)
29. D. Patidar, K.S. Rathore, N.S. Saxena, K. Sharma, T.P. Sharma, J. Nano. Res. **3**, 97 (2008)
30. H. Kargar, F. Ghasemi, M. Darroudi, Ceram. Int. **41**, 1589 (2015)
31. A. Khorsand Zak, W.H. Abd Majid, M.R. Mahmoudian, M. Darroudi, R. Yousefi, Adv. Powder Technol. **24**, 618 (2013)
32. V. Ramasamy, V. Mohana, V. Rajendran, OpenNano **3**, 38 (2018)
33. H. Zhu, J. Xu, Y. Yichuan, Z. Wang, Y. Gao, W. Liu, H. Yin, J. Colloid Interface Sci. **508**, 1 (2017)
34. A.A. Mohamed, A. Fouda, M.A. Abdel-Rahman, S.E.-D. Hassan, M.S. El-Gamal, S.S. Salem, T.I. Shaheen, Biocatal. Agric. Biotechnol. **19**, 101103 (2019)
35. P. Sharma, A.B. Jha, R.S. Dubey, M. Pessarakli, J. Bot. **2012**, 1 (2012)
36. G. Seong, M. Dejhosseini, T. Adschiri, Appl. Catal. B **550**, 284 (2018)
37. A. Fouda, G. Abdel-Maksoud, M.A. Abdel-Rahman, A.M. Eid, M.G. Barghoth, M.A.-H. El-Sadany, Cellulose **26**, 6583 (2019)
38. O. Zuas, H. Abimanyu, W. Wibowo, Pro. App. Cer. **8**, 39 (2014)
39. Y. Tao, F.H. Gong, H. Wang, H.P. Wu, G.L. Tao, Mater. Chem. Phys. **112**, 973 (2008)
40. A. Muthuvel, K. Adavallan, K. Balamurugan, N. Krishnakumar, Biom. Prev. Nutr. **4**, 325 (2014)
41. J. Liqiang, Q. Yichun, W. Baiqi, L. Shudan, J. Baojiang, Y. Libin, F. Wei, F. Honggang, S. Jiazhong, Sol. Energy Mat. Sol. C. **90**, 1773 (2006)
42. C. Zhang, F. Meng, L. Wang, M. Zhang, Z. Ding, Mater. Lett. **130**, 202 (2014)
43. F. Yuan, B. Liu, Y. Zhang, W.J. Weber, J. Phys. Chem. C **120**, 6625 (2016)
44. Y. Huang, B. Long, M. Tang, Z. Rui, M.-S. Balogun, Y. Tong, H. Ji, Appl. Catal. B **181**, 779 (2016)
45. J. Malleshappa, H. Nagabhushana, S.C. Sharma, Y.S. Vidya, K.S. Anantharaju, S.C. Prashantha, B. Daruka Prasad, K. Raja Naika, K. Lingaraju, B.S. Surendra, Spectrochim. Acta A **149**, 452 (2015)
46. M.S. Irshad, M.H. Aziz, M. Fatima, S.U. Rehman, M. Idrees, S. Rana, F. Shaheen, A. Ahmed, M.Q. Javed, Q. Huang, Mater. Res. Express **6**, 0950a4 (2019)
47. M. Fang, J. Chen, X. Xu, P. Yang, H. Hildebrand, Int. J. Antimicrob. Agents **27**, 513 (2006)
48. F. Javadi, M.E. Taghavizadeh Yazdi, M. Baghani, A. Es-haghi, Mater. Res. Express **6**, 065408 (2019)
49. P. Krishnaveni, L. Priya, G. Annadurai, Res. J. Life Sci. Bioinform. Pharm. Chem. Sci. **5**, 585 (2019)
50. L. Uhl, A. Gerstel, M. Chabalier, S. Dukan, Heliyon **1**, e00049 (2015)
51. K. Gopinath, V. Karthika, C. Sundaravadivelan, S. Gowri, A. Arumugam, J. Nanostructure. Chem. **5**, 295 (2015)
52. S.N. Patil, J.S. Paradeshi, P.B. Chaudhari, S.J. Mishra, B.L. Chaudhari, Appl. Biochem. Biotech. **180**, 638 (2016)